

P. Manimaran* and M. Ganesh Madhan

Numerical Analysis of NTW-SOA for Differential Inline Detector Applications

Abstract: An analysis of Near Travelling Wave-Semiconductor Optical Amplifier (NTW-SOA) is presented to investigate its inline detector performance. The detected voltage is evaluated for various lengths and positions of the electrode along the active region of the device, for input optical power levels ranging from -25 dBm to $+5$ dBm. Under optimum conditions, the differential detection scheme shows an improvement of 3.7 dB, 4 dB for 40 mA, 50 mA bias currents respectively at -10 dBm input power, when compared with the best differential inline detection scheme reported in the literature. Further an improvement of 4.3 dB and 5.5 dB are obtained, when compared with the single electrode detection model under similar operating conditions.

Keywords: differential, modelling, inline detection, NTW-SOA

PACS® (2010). 42.55.Px, 42.60.Da, 42.60.Fc, 42.82.-m

***Corresponding author: P. Manimaran:** Department of Electronics Engineering, Madras Institute of Technology Campus, Anna University, Chennai 44, India. E-mail: maran_pm@yahoo.co.in

M. Ganesh Madhan: Department of Electronics Engineering, Madras Institute of Technology Campus, Anna University, Chennai 44, India

1 Introduction

In recent days, Semiconductor Optical Amplifier (SOA) has been gaining importance due to its versatile functionalities and the capability to realize it as photonic integrated circuit (PIC) [1]. There is a growing need to manage the increase in loss budgets associated with optical networks comprising of optical nodes, which facilitate dynamic routing and this could be realized using SOA. The functions of SOA's include optical amplification, wavelength conversion, external modulation, optical switching and inline detection, which could be used in diversified optical communication networks. Inline detection and amplification can be done using SOA which eliminates the need for optical to electrical (O-E) and electrical to optical (E-O) conversions.

The key feature, namely simultaneous amplification and detection in NTW-SOA was reported by Koai and Olshansky [1]. Further studies, showed that two section differential scheme provides improvement in detected voltage [2]. The multifunctional capabilities of NTW-SOA was investigated by Eliseev et al. [3]. A detailed study on the in line detection function was carried out for optical signals with dc component preservation in NT-SOA structure, under single, two and three electrode mechanism, was reported by Rampone et al. [4]. It was proved that the device with three electrode structure under differential mode gave better results than the two electrode structure. As theoretical analysis of SOA's provide detailed understanding and optimization of device operation, various modeling approaches were developed [5]. Among them, the rate equation model, traveling wave model, transmission line model and equivalent circuit approach were important [6, 7].

In the equivalent circuit approach for the analysis of SOA based in line detector, a bi section and mean values for carrier and signal photon densities were used [10]. Coupled differential equations form the basis for the analysis of the detector performance in most of the literature [4]. A detailed model involving more number of sections and Fermi level based approach to calculate the overall gain and carrier density, could be more useful for analysis of inline detection. Moreover computation of the spatial variations of carrier, signal and ASE densities inside SOA could help in fixing the optimum electrode length and position along the device. An $1.55 \mu\text{m}$ wideband model for TWSOA reported by Connelly, incorporates all the parameters of optical amplifier and gives a detailed spatial variations of signal, carrier density and both forward and reverses traveling ASE [8]. Further, it also provides the output signal power, noise figure and ASE spectrum and its influence on material gain and other operating conditions. We use this wideband steady state model for evaluation of voltage developed along the length of device. As the carrier density along the cavity length varies in a nonuniform fashion, the detected voltage also varies accordingly. Introducing electrodes of appropriate lengths at unique locations of the cavity may improve the detection process significantly. Hence the effect of length of the electrodes on the detected voltage in SOA is studied

and compared with the available reports of two and three electrode structures. Further optimum length and position of electrodes for maximum detected voltage are determined.

2 Modeling

The device considered for this work is a 1.55 μm InP-In_xGa_{1-x}As_yP_{1-y}, buried ridge stripe TW-SOA with linear tapering from the centre to zero width at each end. This structure is chosen to provide improved coupling for single mode optical fiber. The following rate equation provides the carrier density developed spacially along the entire length of the active region of the device, which incorporates the forward and reverse traveling signal as well as ASE.

$$\frac{dn(z)}{dt} = \frac{I}{edLW} - R(n(z)) - \frac{\Gamma}{dw} \left\{ \sum_{k=1}^{N_s} g_m(v_k, n(z)) (N_{sk}^+(z) + N_{sk}^-(z)) \right\} - \frac{2\Gamma}{dw} \left\{ \sum_{k=1}^{N_m-1} g_m(v_k, n(z)) K_j((N_j^+(z) + N_j^-(z))) \right\} \quad (1)$$

where

$R(n(z))$ – Recombination rate,

$N_{sk}^+(z)$ – signal photon rate in positive z direction,

$N_{sk}^-(z)$ – signal photon rate in negative z direction

$N_j^+(z)$ – spontaneous emission photon rate for TE mode

$N_j^-(z)$ – spontaneous emission photon rate for TM mode.

The various mechanisms leading to change in carrier density in the active region such as the injected current, spontaneous radiative and non-radiative recombination, stimulated recombination by the signal and ASE photons and augur recombination of carriers are included as in (1).

A detailed material gain (g_m) calculation incorporating the Fermi Dirac distributions in the conduction and valence band is considered for analysis. The carrier density variation due to band gap change is also dealt in the model.

The material gain coefficient of the semiconductor medium is given as

$$g_m = g_m' - g_m'' \quad (2)$$

where g_m' is the gain coefficient and g_m'' the absorption coefficient, which are given by

$$g_m' = \frac{c^2}{4\sqrt{2}\pi^{3/2}n_1^2\tau v^2} \left(\frac{2m_e m_{hh}}{\hbar(m_e + m_{hh})} \right)^{3/2} \times \sqrt{v - \frac{E_g(n)}{h}} f_c(v) (1 - f_v(v)) \quad (3)$$

$$g_m'' = \frac{c^2}{4\sqrt{2}\pi^{3/2}n_1^2\tau v^2} \left(\frac{2m_e m_{hh}}{\hbar(m_e + m_{hh})} \right)^{3/2} \times \sqrt{v - \frac{E_g(n)}{h}} (1 - f_c(v)) f_v(v) \quad (4)$$

The Fermi-Dirac distributions of conduction and valence band of the active region material are given by the usual relations. The parameters used in the above equations are as follows. 'c' is the speed of light, 'v' is the optical frequency, 'τ' is the radiative carrier recombination lifetime, 'n' is the conduction band carrier density, 'f_c(v)' is the Fermi-Dirac distribution in the conduction band, 'f_v(v)' is the Fermi-Dirac distribution in the valence band and 'E_g(n)' is the band gap energy.

The amplification of the signal photons takes place along the length of the device and also gives rise to ASE photons leading to a variation in the carrier density. This in turn changes the voltage along the active region and is observed by the difference in the quasi-Fermi levels given by the following equation [8]

$$V_\phi(z) = E_{fc} - E_{fv} \quad (5)$$

This approach offers more precise value of the detected voltage compared to the existing schemes [4]. The optical signals entering the front facet are amplified and exit at the opposite facet. The voltage developed due to carrier density variations along the length of SOA at different power levels, for various bias currents are determined under the single electrode and differential detection schemes. The parameters used in the simulation are listed in Table 1.

3 Simulation results and analysis

3.1 Device characteristics

Numerical solutions of (1)–(4) are obtained using Finite difference solutions and the carrier densities are evaluated along the length of the cavity, for different optical input powers. The total length of the NTW-SOA is divided into 100 sections for the analysis. The carrier density profile obtained is similar to the observations of Connelly

Table 1: TWSOA parameters [8]

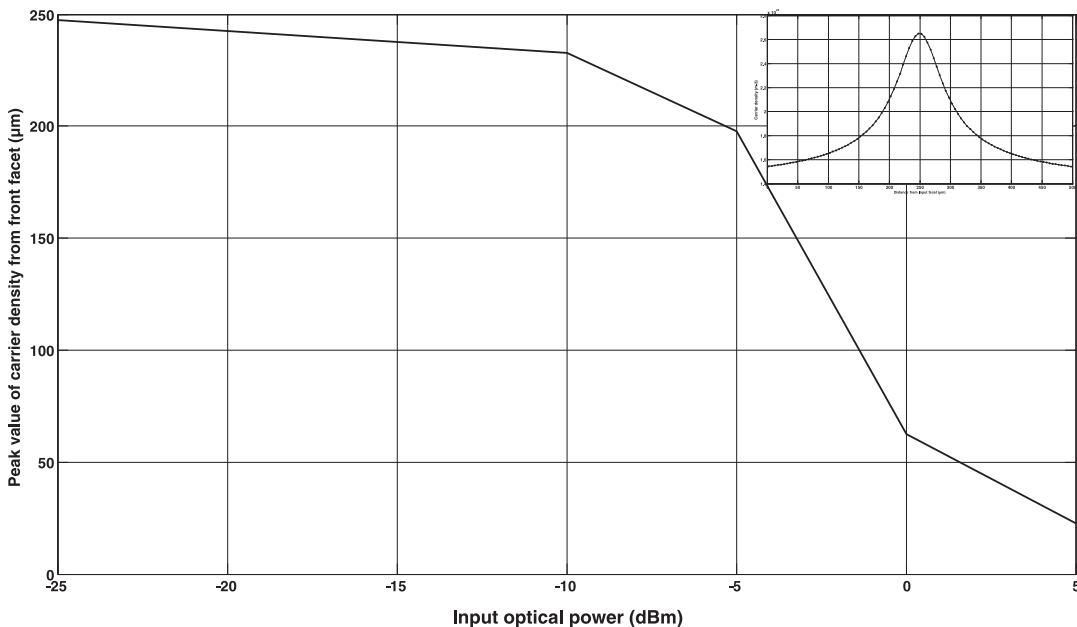
Symbol	Parameter	Value
L_c	Central active region length	450 μm
L_t	Tapered active region length	50 μm
d	Active region thickness	0.4 μm
W	Central active region width	0.4 μm
Γ	Confinement factor	0.45
K_g	Band gap shrinkage coefficient	$0.9 \cdot 10^{-10}$ eVm
n_1	InGaAsP active region refractive index	3.22
n_2	InP region refractive index	3.167
dn_1/dn	Active region RI change with n	$-1.8 \cdot 10^{-26}$ m ⁻³
n_{eq0}	Equivalent RI at n = 0	3.22
dn_{eq}/dn	Equivalent RI of active region change	$-1.34 \cdot 10^{-26}$ m ⁻³
$\eta_{in} \eta_{out}$	Input and output coupling loss	3 dB
R_1, R_2	Input, output Reflectivity	$5 \cdot 10^{-5}$
K_0	Independent loss coefficient	6200 m ⁻¹
K_1	Dependent loss coefficient	7500 m ²
A_{rad}	Linear radiative recombination coefficient	$1 \cdot 10^7$ s ⁻¹
B_{rad}	Bimolecular radiative recombination coefficient	$5.6 \cdot 10^{-16}$ m ³ s ⁻¹
C_{aug}	Auger recombination coefficient	$3 \cdot 10^{-41}$ m ⁶ s ⁻¹
D_{leak}	Leakage recombination coefficient	$0.0 \cdot 10^{-48}$ m ^{13.5} s ⁻¹
A_{nrad}	Linear nonradiative recombination coefficient	$3.5 \cdot 10^8$ s ⁻¹
N_T	Carrier density at threshold	$4.5 \cdot 10^{22}$ /m ³

etal [8] and hence validates our procedure. This behaviour is shown as an inset in Fig. 1. It is seen that for given values of optical input powers the carrier density shows a maximum around the centre of the active region length. The position corresponding to the peaks of the carrier densities are plotted in Fig. 1 under various input powers. It is observed that for power levels until -5 dBm, the positions of the peak values lie between 250–200 μm , from the front facet of the device.

The voltage profile determined and plotted in Fig. 2 gives a better idea to decide the length and position of the detection electrodes for better response. A reversal in phase is observed in the spatial profile of the voltage detected along the length of the device as reported in literature [1, 9].

3.2 Conventional single electrode detection scheme

A full length electrode for the entire length of 500 μm is used to detect the optical signal and it is obtained by averaging the voltage produced along the entire length of the SOA. Fig. 3 shows the detected voltages for their respective input optical powers at different bias currents. It is clear from the graph that above 50 mA bias current, the detected voltage doesn't improve. Hence we observe that higher bias current may not provide enhancement in detected voltage.

**Fig. 1:** Peak positions of the carrier density for different power levels of the TWSOA

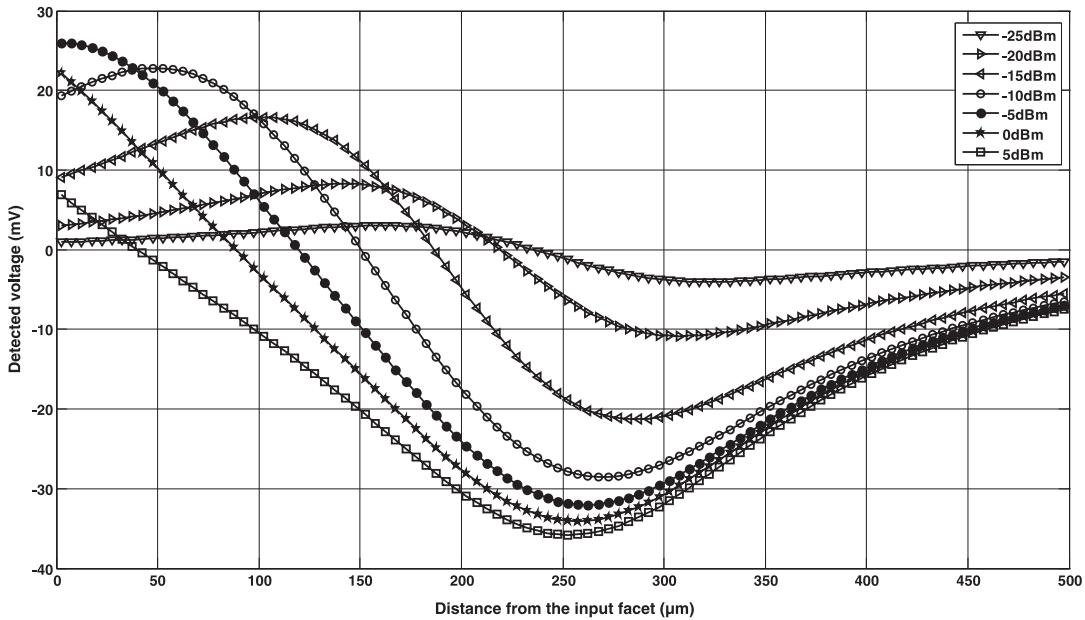


Fig. 2: Spatial variation of detected voltage for 50 mA bias current

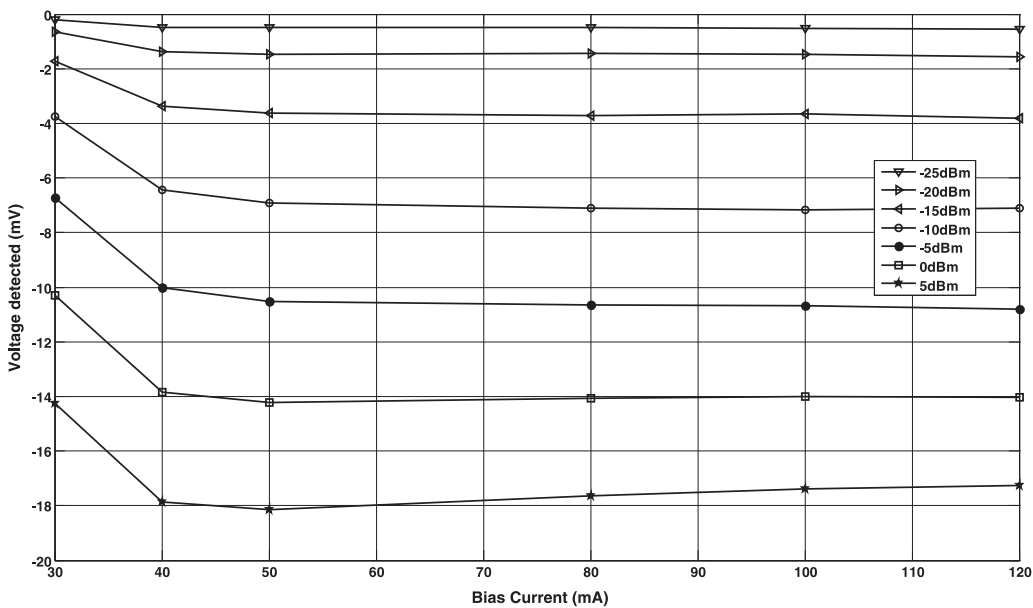


Fig. 3: Single electrode detected voltage as a function of bias currents

3.3 Differential detection scheme

$$V_{d\phi}(z) = V_{s\phi}(z) - V_{l\phi}(z) \tag{9}$$

The differential detection arrangement consists of two electrodes namely reference and signal electrode (Fig. 4). However the entire active region is electrically pumped as discussed in the literature [4]. The detected voltage is the difference between the voltages developed between the two electrodes and as given by the following equation

In this analysis, the signal electrode is kept at a constant length of 200 μm at a location 300–500 μm from the front facet. This could be justified as there is not much of variation in spatial profile (Fig. 2) of the detected voltage in this region. The reference electrode length is varied and positioned at different locations from input facet, due to

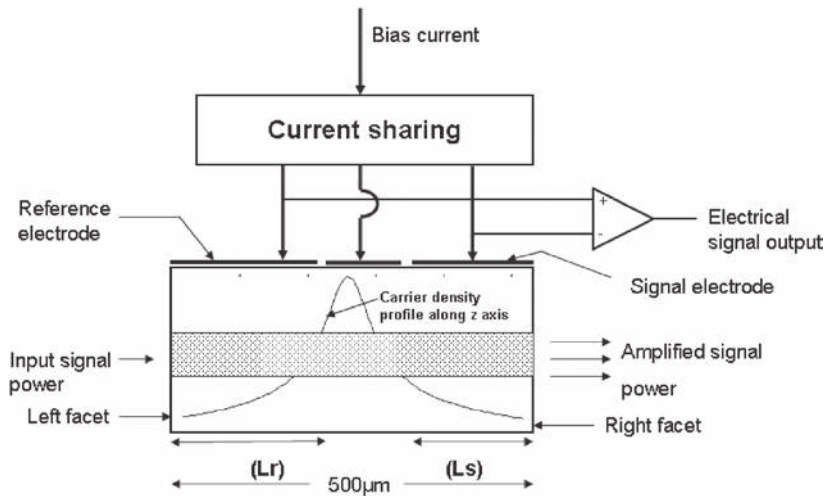


Fig. 4: Differential detection scheme

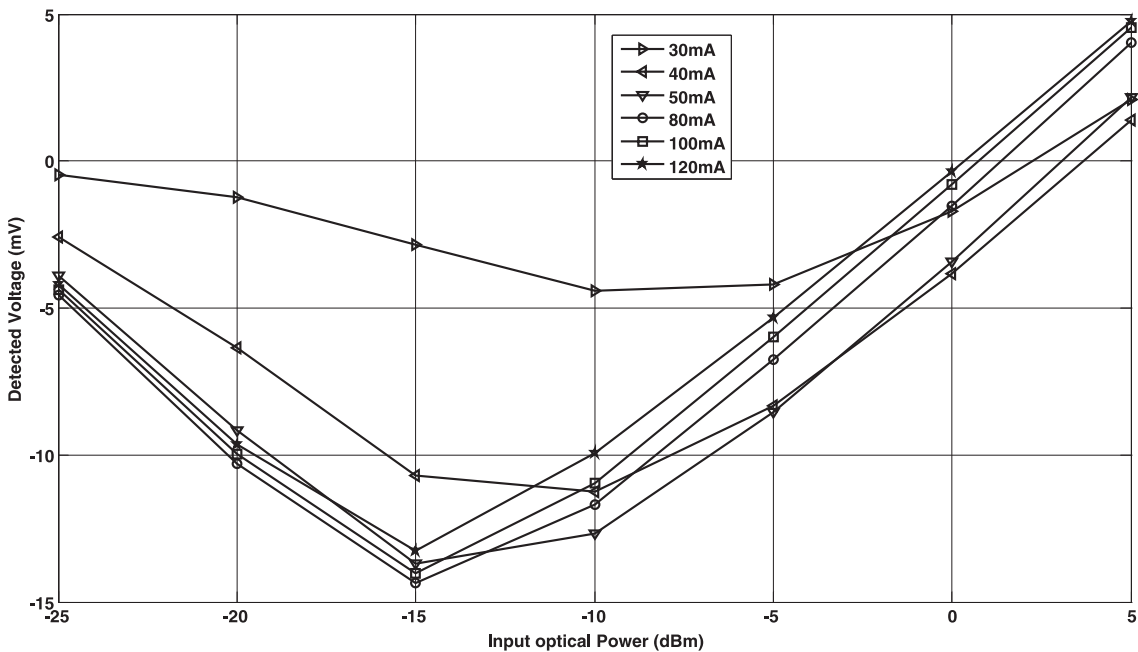


Fig. 5: Differential detected Voltage as a function of input optical power ($L_r = 300 \mu\text{m}$)

the fact that the variations in detected voltage are observed in 1–300 μm length from the front facet. Simulations are carried out under these conditions and the detected voltage and responsivity are plotted under various input powers.

Figure 5 shows the detected voltages for two section SOA, with reference electrode length of 300 μm , where a maximum value of 14 mV is obtained at 80 mA bias, -15 dBm input power. It is also seen that the detected voltage undergoes a phase reversal around 0 dBm. Further

the detected voltage does not improve for higher bias current as well as input powers.

The responsivity (Fig. 6) is found to be low for the higher input powers as the detected voltage variation is less. However, the responsivity is found to be higher for lower optical signal powers. These observations are exactly coinciding with the experimental results of Rampone et al. [4] and therefore validating our simulations. An analysis is made by varying the length of reference electrode from 300 μm to 100 μm as discussed

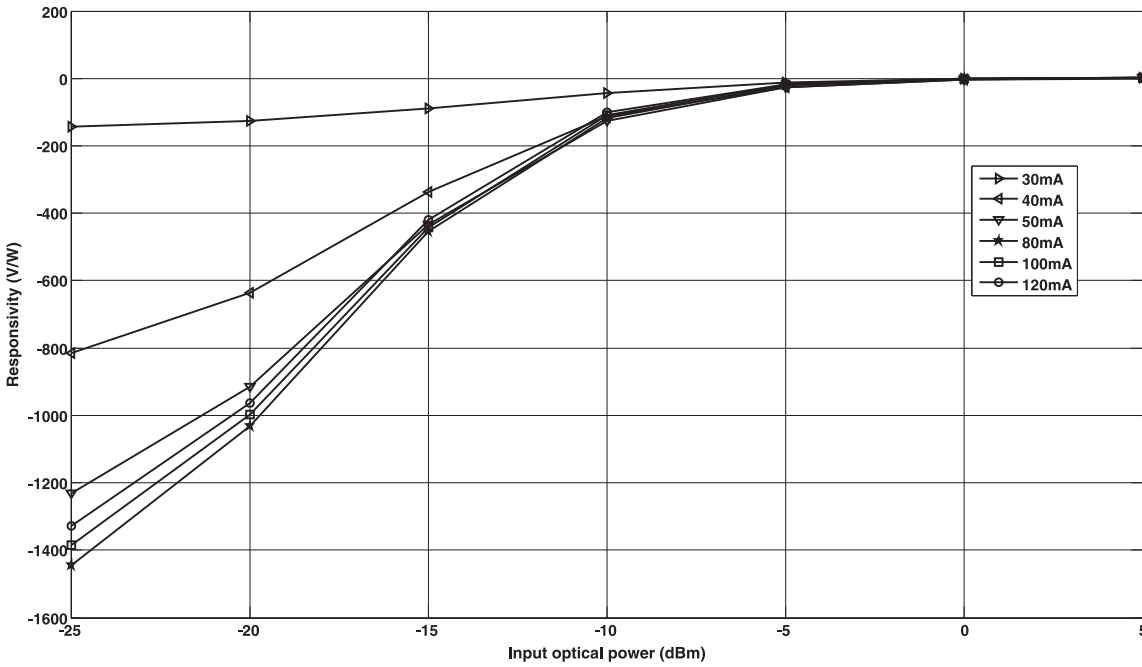


Fig. 6: Responsivity of differential detection as a function of input optical power ($L_r = 300 \mu\text{m}$)

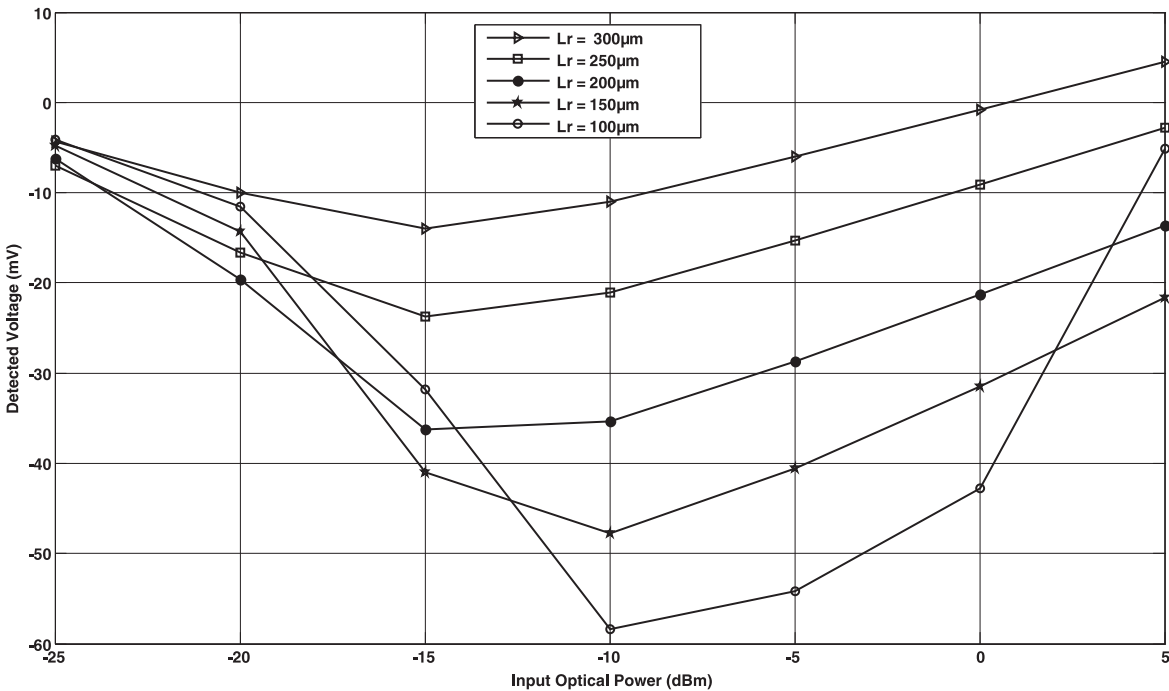


Fig. 7: Detected voltage of as a function of input optical power for different length of reference electrodes

earlier. In all the cases, the reference electrode is positioned at the left facet of the TWSOA. Figs. 7 and 8 show the detected voltage and responsivity, for a bias current of 100 mA. Table 2 provides the values of detected voltage

and responsivity for -10 dBm and -20 dBm input powers. The reference electrode length of $300 \mu\text{m}$, gives a detected voltage of 10.97 mV at -10 dBm and shows a responsivity of 109.7 V/W . These values are better than the single elec-

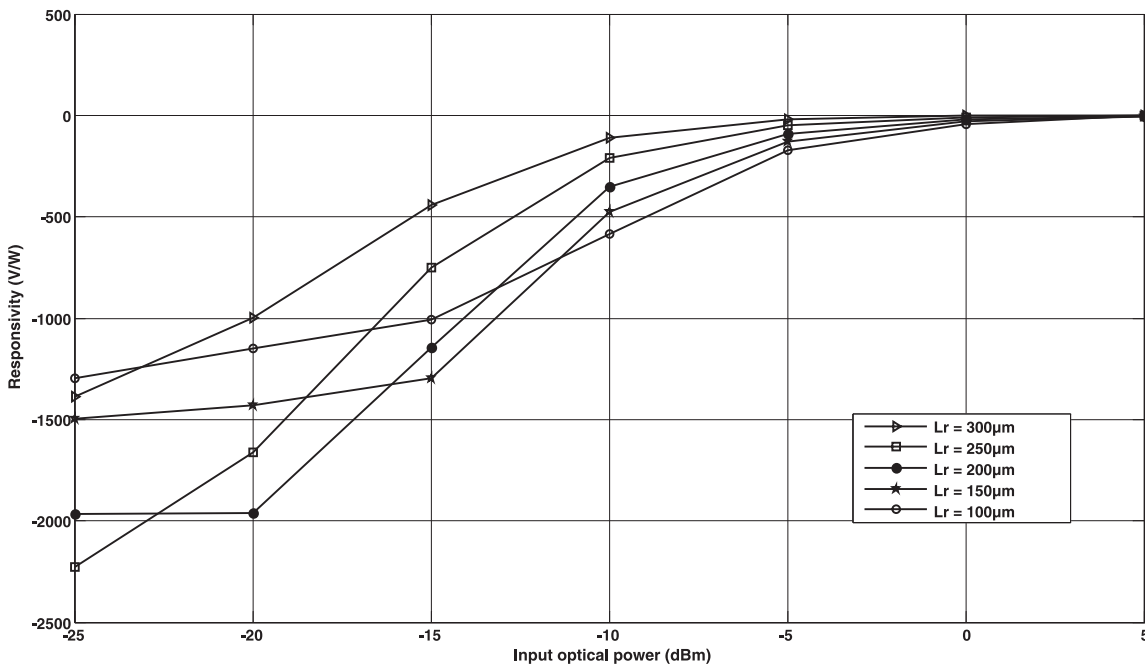


Fig. 8: Responsivity of differential detection as a function of input optical power for different lengths of reference electrode.

Table 2: Maximum detected voltage and responsivity for different electrode lengths (100 mA of bias current)

Length of the Reference Electrode L_r (μm)	Detected voltage (mV)		Responsivity (V/W)	
	-10 dBm	-20 dBm	-10 dBm	-20 dBm
300	10.97	9.98	109.7	998.3
250	21.06	11.51	210.6	1662
200	35.36	14.31	353.6	1962
150	47.74	16.62	477.4	1431
100	58.41	19.62	584.1	1151

trode scheme. The structure with L_r of 250 μm provides still higher voltage, which is almost twice than that of previous case and also shows good responsivity. For reference electrode length of 200 μm , the detected voltage rises up to 35.36 mV for -10 dBm and responsivity upto 1962 V/W for -20 dBm, which is the maximum, when compared to other lengths. It is also clear that electrode positions at (1–150 μm) and (1–100 μm) have higher detected voltage. But the responsivity is poor.

From the above analysis, it is understood that the electrode structure with reference electrode length of 200 μm positioned at the front facet, is found to be the optimum position for differential detection, which has significantly higher detected voltage (Fig. 9) along with

maximum responsivity (Fig. 10). In this position, higher input powers also shows a good distinction in terms of detected voltage and responsivity. Further higher bias currents lead to improvement in detected voltage. Table 3 reveals the detected voltage levels for various bias currents for different electrode lengths as examined. It is clear that the optimum position based scheme shows a better performance than other schemes and found to have an improvement of 3.7 dB and 4 dB for 40 mA and 50 mA bias currents at -10 dBm, with respect to the three section model reported. Further an improvement of 4.3 dB and 5.5 dB is observed when compared with the single electrode scheme. However for lower bias currents, this approach shows a marginal improvement.

4 Conclusion

An in depth analysis of both single section and differential detection based on the electrode length is reported in this paper. It is found that reference electrode of 200 μm length positioned at the input facet and signal electrode (200 μm) fixed at the right facet, proves to be efficient compared to other electrode positions evaluated and also with the single section detection model. The optimized differential electrode scheme is found to provide an improvement of 3.7 dB and 4 dB for 40 mA and 50 mA bias currents at

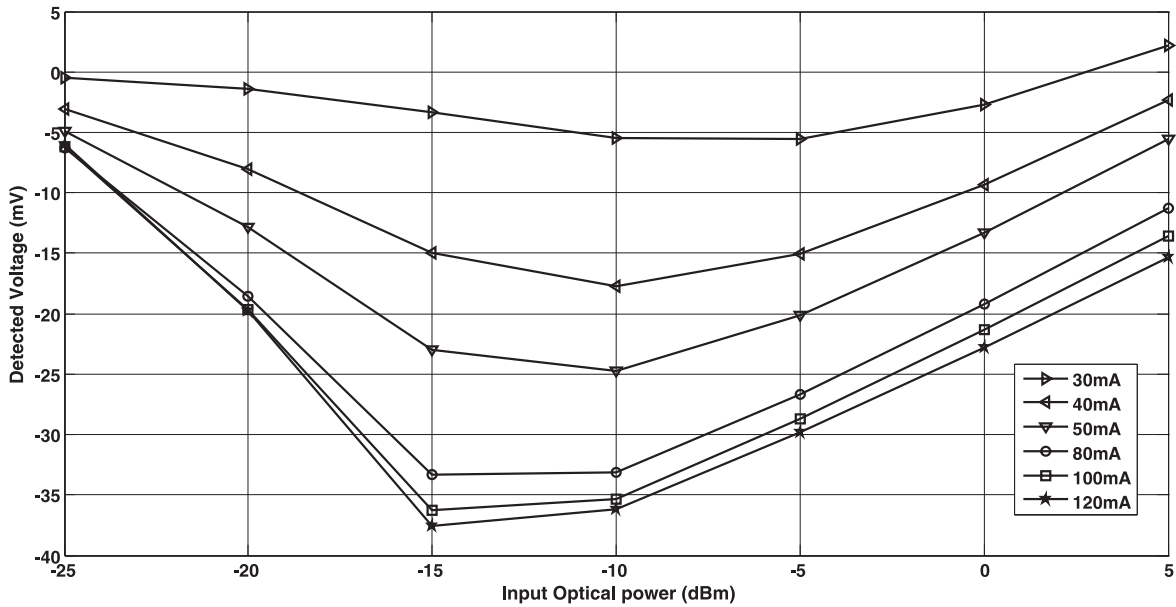


Fig. 9: Differential detected voltage for 200 μm reference electrode length at different bias currents.

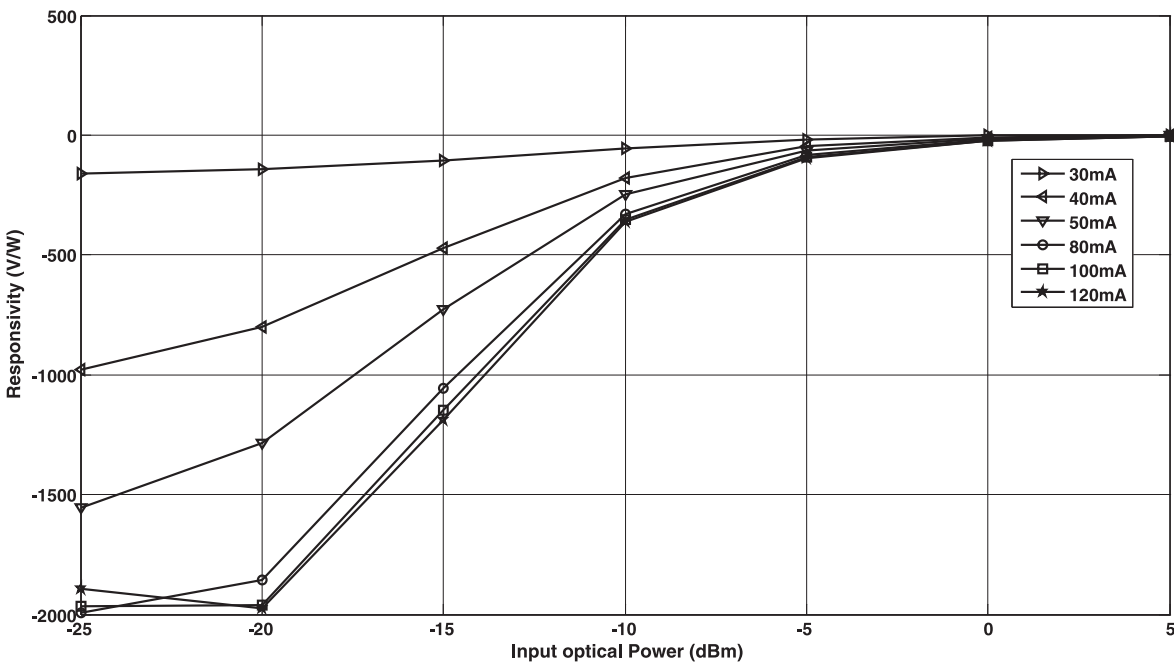


Fig. 10: Responsivity of differential detection as a function of input optical power

-10 dBm input power, with respect to the three section model reported in the literature. Further an improvement of 4.3 dB and 5.5 dB is observed when compared with the single electrode detection model.

Acknowledgments: The authors gratefully acknowledge Department of Science and Technology (DST), Govt of

India, New Delhi for providing financial support to carry out this research work under PURSE scheme. One of the authors, Mr. P. Manimaran is thankful to Department of Science and Technology (DST), Govt of India, New Delhi for the award of DST-PURSE fellowship.

Received: February 22, 2013. Accepted: May 22, 2013.

Table 3: Comparison of detected voltage of various detection schemes at -10 dBm input optical power

Bias current (mA)	Detected voltage (mV)		
	Single full length electrode	Optimized differential electrode scheme	Differential electrode [4]
30	4	5.5	3.4
40	6.5	17.76	7.5
50	7	24.77	10

References

- [1] K.T. Koai and R. Olshansky, "Simultaneous Optical Amplification, Detection, and Transmission Using In-Line Semiconductor Laser Amplifiers", *IEEE Photonics Tech. Lett.*, Vol. 4, No. 5, pp. 441–443, 1992.
- [2] R.M. Fortenberry, A.J. Lowery and R.S. Tucker, "Up to 16 dB improvement in detected voltage using two section semiconductor optical amplifier detector", *Electronics Letters*, 28(5), 474–475, 1992.
- [3] Peter G. Eliseev and Vu Van Luc, "Semiconductor optical amplifiers: multifunctional possibilities, photo response and phase shift properties", *Pure Appl. Opt.*, Vol. 4, pp. 295–313, 1995.
- [4] Thierry Rampone, Hong-Wu Li and Ammar Sharaiha, "Semiconductor Optical Amplifier Used as an In-Line Detector with the Signal DC-Component Conversation", *IEEE J. Light Wave Technology*, Vol. 16, No. 7, pp. 1295–1301, 1998.
- [5] H. Ghaffouri Shiraz, "The principles of semiconductor laser diodes and amplifiers", Imperial College Press, London, 2004.
- [6] A.J. Lowery, "Modeling spectral effects of dynamic saturation in semiconductor laser amplifiers using the transmission line laser model", *IEEE Proc, Part. J*, Vol. 36, No. 6, pp. 320–324, 1989.
- [7] M. Ganesh Madhan and R. Neelakandan, "An improved transmission line laser model for multimode laser diodes incorporating thermal effects", *Opt. Quant. Electron*, Vol. 40, No. 8, pp. 535–550, 2008.
- [8] Michael J. Connelly, "Wideband Semiconductor Optical Amplifier Steady-State Numerical Model", *IEEE, JQE*, Vol. 37, No. 3, 2001.
- [9] A. Sharaiha and M. Guegan, "Analysis of the sign reversal of the photo detected signal response in a multielectrode semiconductor optical amplifier", *IEEE J. of Lightwave Technology*, Vol. 19, No. 8, pp. 1185–1193, 2001.
- [10] Eszter Udvary and Tibor Berceli, "Semiconductor Optical Amplifier for Detection Function in Radio Over Fiber systems", *IEEE J. Lightwave Technology*, Vol. 26, No. 15, pp. 2563–2570, 2008.

